Nanoscale

Fundamental Scaling Laws for the Direct-Write Chemical Vapor Deposition of Nanoscale Features: Modeling Mass Transport Around a Translating Nanonozzle

Journal:	*Nanoscale*
Manuscript ID	NR-ART-12-2018-010366
Article Type:	Paper
Date Submitted by the Author:	22-Dec-2018
Complete List of Authors:	Drahushuk, Lee; Massachusetts Institute of Technology, Chemical Engineering Govind Rajan, Ananth; MIT, Chemical Engineering Strano, Michael; MIT, Chemical Engineering;

Fundamental Scaling Laws for the Direct-Write Chemical Vapor Deposition of Nanoscale Features: Modeling Mass Transport Around a Translating Nanonozzle

*Lee W. Drahushuk,‡ Ananth Govind Rajan‡ and Michael S. Strano**

Massachusetts Institute of Technology, Department of Chemical Engineering,

Cambridge, MA 02139 USA

*Corresponding author: strano@mit.edu

‡ L.W.D. and A.G.R. contributed equally.

Keywords: atomically precise manufacturing, nanoscale precision, nanoribbon, synthesis, molecular printing, CVD

ABSTRACT

The nanometer placement of nanomaterials, such as, nanoribbons and nanotubes, at a specific pitch and orientation on a surface, remains an unsolved fundamental problem in nanotechnology. In this work, we introduce and analyze the concept of a direct-write chemical vapor deposition (CVD) system that enables the in-place synthesis of such structures with control over orientation and characteristic features. A nanometer scale pore or conduit, called the nanonozzle, delivers precursor gases for CVD locally on a substrate, with spatial translation of either the nozzle or the substrate to enable a novel direct write (DW) tool. We analyze the nozzle under conditions where it delivers reactants to a substrate while translating at a constant velocity over the surface at a fixed reaction temperature. We formulate and solve a multi-phase three-dimensional reaction and diffusion model of the direct-write operation, and evaluate specific analytically-solvable limits to determine the allowable operating conditions, including pore dimensions, reactant flow rates, and nozzle translation speed. A Buckingham Π analysis identifies six dimensionless quantities crucial for the design and operation of the direct-write synthesis process. Importantly, we derive and validate what we call the *ribbon extension inequality* that brackets the allowable nozzle velocity relative to the CVD growth rate – a key constraint to enabling direct-write operation. Lastly, we include a practical analysis using attainable values towards the experimental design of such a system, building the nozzle around a commercially available near-field scanning optical microscopy (NSOM) tip as a feasible example.

INTRODUCTION

The synthesis and placement of nanomaterials with nanometer or Angstrom scale precision[1–4] remains a longstanding, but largely unsolved challenge, in nanotechnology. The extreme limit of this challenge has been called atomically precise manufacturing (APM) in the literature.[5–7] There exists significant interest in developing electronic components from graphene and other 2D materials in their nanoribbon forms, which are predicted[8] and shown[9,10] to have favorable electronic bandgaps for digital electronic applications, unlike unmodified graphene. Because of the edge variance of lithographic methods, it becomes increasingly difficult to create small ribbon widths or nanowire diameters as the characteristic length decreases.[11] Moreover, it has been noted that to achieve high electron mobilities in nanoribbon structures, edge defects must be suppressed.[12] This prompts an exploration of fabrication methods that could scale to atomic-level precision, unlike conventional, subtractive lithographies.[13] There have been several efforts to modify existing approaches to reach the APM scale, including: (i) electron-beam lithography,[14] (ii) electric or magnetic field-driven alignment of nanowires,[15] (iii) chemical synthesis using thermally-activated atomic force microscopy tips,[16,17] and (iv) DNA origami.[18] However, low throughput and applicability to a limited set of materials have prevented the broad application of these techniques for APM. In this work, we conceptually introduce an alternative concept of direct-write chemical vapor deposition (CVD) as a nanofabrication tool that could potentially scale to APM levels. Our work provides the first mathematical modeling framework for such an approach and examines the conditions of its feasibility. We develop the concept of a spatially-translating nanometer scale pore or conduit through which precursor gases for

CVD are delivered to enable a novel direct-write (DW) tool. Since CVD is a widely utilized technique for the synthesis of a broad range of materials, ranging from nanotubes[19] and two-dimensional materials,[20] to metals[21] and semiconductors,[22] this technique offers synthetic access to a wide range of target nanomaterials and structures.

Existing direct-write lithographic methods cannot achieve the requisite spatial resolution for a wide range of applications. Electron-beam (e-beam) lithography, which uses a focused beam of electrons to create desired features on a surface that is coated with an electron-sensitive film, has conventionally allowed resolutions up to 10 nm,[23] though recent advances have pushed the resolution limit to around 1 nm in certain cases.[14] E-beam lithography is often used for nanopatterning of surfaces,[24] including nanoribbons.[25] However, the use of an electron-sensitive film (the resist) limits the applicability of this method. Further, nanoribbons synthesized using lithographic techniques typically lose their conductance due to lack of control over the resulting edge structure. Other lithography avenues that have been explored for nanopatterning include chemical synthesis using thermally-activated atomic force microscopy tips, known as "dip-pen nanolithography". While this technique is useful for depositing material which is compatible as an ink,[26] it is not well suited for controlled delivery of precursors for higher temperature CVD reactions that lead to pristine lattices and edges. Indeed, dip-pen nanolithography has primarily been utilized for patterning polymeric surfaces, which are best handled at comparatively lower temperatures.[16,17]

The controlled placement of nanometer-scale materials on a surface has also been explored, such as the alignment of nanowires along preferred directions using electric[27]

and magnetic[28] fields. However, such alignment techniques do not necessarily enable control of the spacing or pitch between nanowires with nanometer precision. Moreover, the use of magnetic fields limits the technique to magnetic substrates. DNA origami is another promising technique to create nanoscale shapes and patterns which are biologically compatible.[29] Recently, DNA origami was utilized to adjust the distance between two fluorescent molecules with sub-nanometer precision.[18] However, the main challenges facing the use of this technique are low yield and production scale, and the cost of synthetic DNA.[30]

In this work, we address the lack of scalable and widely applicable methods for achieving nanometer-scale precision in the orientation and placement of nanomaterials. We introduce and analyze the concept of direct-write CVD, formulating the foundational scaling laws that dictate its successful design and operation. Our conception of the direct-write CVD reactor involves a translating nanoscale nozzle (henceforth termed a *nanonozzle*) to achieve nanoscale patterning. A nanonozzle has the ability to localize a small flux of precursor molecules, which diffuse from the tip of the nanonozzle as an efflux. Using this aspect to localize a reagent for nanoribbon growth yields distinct results compared to reactions occurring in the bulk phase. In the past, researchers have utilized "nanojets" as an energetic plasma to etch away a surface to form a desired nanoscale structure,[31] or laser ablation to release and deliver larger molecules locally.[32] However, the key aspect of the nanonozzle concept explored in this work is that the structure and precision of the structures grown are derived from the moving local delivery and diffusion of the reagent to create a concentration gradient that enables nanoscale patterning. We use continuum simulations to explore the relevant process

parameters and systemic considerations for the design of a nanonozzle system capable of growing a nanoribbon using a CVD reaction. Finally, we compare our results with analytical models which enable us to bracket the performance of the nanonozzle.

RESULTS AND DISCUSSION

The Nanonozzle Concept. A conceptual illustration of a nanonozzle is depicted in Figure 1(a,b), wherein a plume of reagent originates from a single walled carbon nanotube (the nanonozzle) translating at a fixed velocity, and gives rise to a nanoribbon or nanostructure with known growth kinetics on a planar substrate. In Figure 1(c), we illustrate an engineering schematic of the envisioned nanonozzle. Specifically, a nozzle of radius r, translating at velocity v, is placed at a distance h from a substrate with the growing ribbon. The reagent, with a bulk, vapor phase diffusivity D, is emitted from the nozzle mouth at a flow rate Q. We simplify the growth to first-order reaction kinetics, with a rate constant k, and growth occurring at the edge of the growing structure, leading to consumption of the growth reagent and extension of the ribbon, which has a specific area (*i.e.*, material area per unit mass) σ. In future work, a more detailed calculation model could incorporate multiple growth precursors and exact growth kinetics based on mechanisms such as the Langmuir-Hinshelwood model. The growing ribbon possesses a location-dependent width W at a distance x from the nanonozzle. **Table 1** summarizes the physical variables relevant to the operation of the conceived nanonozzle system.

In terms of the boundary conditions (formulated below), far away from the nanonozzle, in the x and y directions, the concentration of the precursor is zero. In the z direction, a no flux boundary condition is applied at the growth substrate and at the top of

the of the system. The competition between reaction and diffusion of the growth reagent creates a concentration gradient, which favors growth close to the nozzle, thereby ensuring that the structure does not grow significantly at locations far away from the nozzle. The surface growth and kinetics are modeled based on graphene synthesis on a catalytic copper surface, which occurs by first nucleating a seed crystal of graphene, with subsequent growth outward from the edges in a monolayer. In the following analysis, we assume that the starting seed crystal exists and that a ribbon grows as a monolayer extending from the seed crystal. Future work could explore the growth of multilayered materials using the nanonozzle. We assume that the only reaction that occurs is reagent addition to the edges of the ribbon and that the nucleation of additional seeds is negligible. Note that, in practice, the seed(s) nucleated on the substrate could be readily located using a grid of lithographic markers deposited prior to the nucleation step. Since, as explained later, a potential candidate for the nanonozzle is a near-field scanning optical microscopy (NSOM) tip, we anticipate that imaging capabilities would be built into the direct-write framework, thereby making it easy to position the nozzle at any desired location.

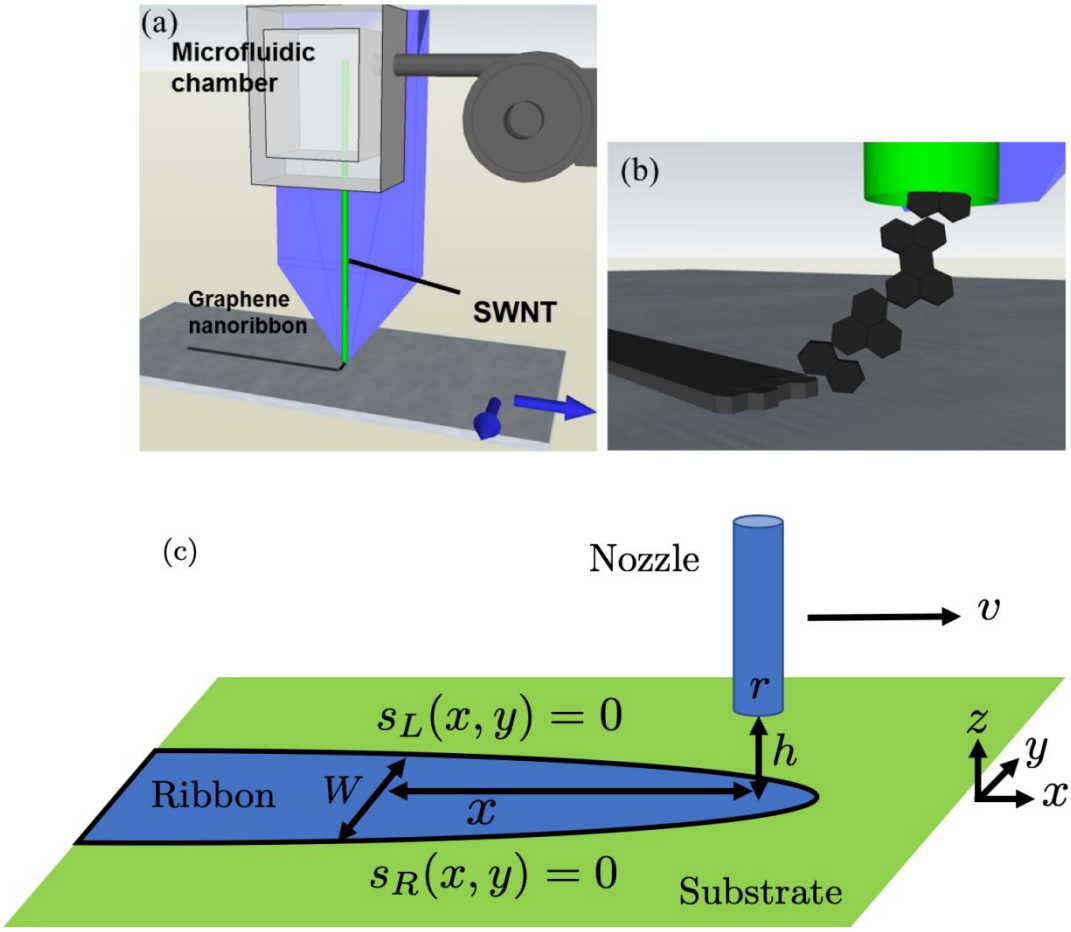

Figure 1. (a) Idealized illustration of graphene nanoribbon growth by a nanonozzle formed from a single walled carbon nanotube (SWNT) that delivers reagent to the site of the growing nanoribbon. (b) Zoomed-in image depicting molecular species emanating from the nozzle mouth and adding to the edge of the growing ribbon. (c) Engineering diagram of the nanonozzle setup with a ribbon growing on a substrate. The nozzle, which translates at a velocity v, has a radius r and is placed at a distance h from the substrate. The location-dependent ribbon width, W, at a distance x from the nozzle is indicated. The growth substrate is located at $z=0$. The left and right edges of the growth ribbon, represented using mathematical functions, $s_L(x,y)=0$ and $s_R(x,y)=0$, respectively, are also shown.

Table 1. Summary of the relevant physical parameters and variables in the nanonozzle system, along with their SI units.

	Description	**SI units**
D	Diffusion constant	$m^2\ s^{-1}$
k	Edge reaction constant	$m^2\ s^{-1}$
σ	Material area per mass	$m^2\ mol^{-1}$
h	Nozzle outlet height	m
Q	Reagent flow rate out of nozzle	$mol\ s^{-1}$
v	Stage translation velocity	$m\ s^{-1}$
r	Nozzle outlet radius	m
x	Distance from the nozzle outlet along surface	m
W	Ribbon width at distance x	m

Nanonozzle Simulations. To explore the concept of a nanonozzle, we developed a simple continuum simulation framework for the system. The example considered is modeled on a monolayer ribbon, growing only at the edges of the existing ribbon, and starting from a seed at the beginning of the simulation. Considering the case of mass transport by diffusion only (the vapor phase is stagnant), we applied the following molar balance equations for the bulk vapor:

$$\frac{\partial C}{\partial t} = D\left(\frac{\partial^2 C}{\partial x^2} + \frac{\partial^2 C}{\partial y^2} + \frac{\partial^2 C}{\partial z^2}\right) + gen \qquad (1)$$

where $C(x,y,z,t)$ represents the location- and time-dependent concentration of the growth reagent in the vapor phase, x, y, and z represent the coordinates of a point in space (note that the growth substrate is located at $z = 0$), t denotes time, D is the diffusivity of the growth reagent, and *gen* represents a molar generation term per unit volume. The generation term is equal to the reagent flow rate (Q) at the nozzle outlet (located within

the spatial region $x_{N,\min} \le x \le x_{N,\max}, y_{N,\min} \le y \le y_{N,\max}, z_{N,\min} \le z \le z_{N,\max}$) and zero everywhere else, as follows:

$$gen(x,y,z,t) = \begin{cases} Q; & x_{N,\min} \le x \le x_{N,\max}, \\ & y_{N,\min} \le y \le y_{N,\max}, \\ & z_{N,\min} \le z \le z_{N,\max} \\ 0; & otherwise \end{cases} \quad (2)$$

Note that, as the ribbon grows, the functions $s_L(x,y)$ and $s_R(x,y)$ should be updated to reflect the new left (L) and right (R) boundaries of the ribbon, according to the amount of material consumed from the gas phase in the timestep Δt, and the material area per unit mass, σ:

$$\{y_L \mid s_L(x,y_L) = 0\} = y_L + \sigma k C(x,y_L,0.5\Delta z,t)\Delta t \quad (3)$$

$$\{y_R \mid s_R(x,y_R) = 0\} = y_R - \sigma k C(x,y_R,0.5\Delta z,t)\Delta t \quad (4)$$

In practice, in the simulation, the ribbon boundaries $s_L(x,y)$ and $s_R(x,y)$ are tracked based on an auxiliary variable $R(x,y,t)$ which denotes the ribbon coverage in the pixel centered at location (x,y). If $R(x,y,t) = 0$, it means the ribbon is not yet grown at location (x,y) at time t. On the other hand, if $R(x,y,t) = 1$ it means the ribbon has fully grown in the pixel centered at location (x,y) at time t. Note that $R(x,y,t)$ is incremented during the current timestep, only if the adjoining (either orthogonally or diagonally) pixel(s) have already grown ribbons, according to the following equations:

$$C(x,y_{L/R},0.5\Delta z,t+\Delta t)=\frac{C(x,y_{L/R},0.5\Delta z,t)}{1+\left(\frac{k}{\Delta A}\right)t_{growth}(x,y_{L/R},t)} \quad (5)$$

$$R(x,y_{L/R},t+\Delta t)=R(x,y_{L/R},t)+\frac{\sigma\Delta V}{\Delta A}\left(C(x,y_{L/R},0.5\Delta z,t)-C(x,y_{L/R},0.5\Delta z,t+\Delta t)\right) \quad (6)$$

where $\Delta A=\Delta x\Delta y$ is the area of the pixel (with length Δx and width Δy) at the edge of the growing ribbon, $\Delta V=\Delta x\Delta y\Delta z$ is the volume of the voxel just above the edge of the growing ribbon (with length Δx, width Δy, and height Δz), $C(x,y_{L/R},0.5\Delta z,t)$ is the reagent concentration just above the growth pixel at the beginning of the timestep, and Eq. (5) is written assuming the growth pixel as a well-mixed system (a continuous stirred-tank reactor[33]). Typically, each pixel on the surface has an "available time for ribbon growth", $t_{growth}(x,y_{L/R},t=0)=\Delta t$. Note that, in some cases, it is possible for the growth pixel to completely grow the ribbon using less time than Δt, i.e., $t_{growth}(x,y_{L/R},t)\geq\frac{(1-R(x,y_{L/R},t))\Delta V}{kC_{\min}\sigma\Delta A}$, where $C_{\min}$ is the concentration just above the completely-grown pixel once all the reagent required for growth has been consumed. In such cases, the reagent concentration above the completely-grown pixel is set to $C_{\min}$, as defined below, and the extra "available time for ribbon growth" is transferred to the adjoining pixel, as expressed in Eq. (9):

$$C_{\min}=C(x,y_{L/R},0.5\Delta z,t)-\frac{\Delta A}{\sigma\Delta V}(1-R(x,y_{L/R},t)) \quad (7)$$

$$R(x, y_{L/R}, t + \Delta t) = 1; \quad provided\, C_{\min} \geq 0 \tag{8}$$

$$t_{growth}(x - \Delta x, y_{L/R}, t + \Delta t) = t_{growth}(x - \Delta x, y_{L/R}, t) + \left(\Delta t - \frac{(1 - R(x, y_{L/R}, t))\Delta V}{kC_{\min}\sigma \Delta A} \right) \tag{9}$$

Afterwards, the stage is translated by shifting the ribbon position to match the growth rate at the leading edge, $(x_0, 0)$, of the ribbon to the growth rate at the edges, such that:

$$\{x_0 \mid s_L(x_0, 0) = s_R(x_0, 0) = 0\} = x_0 + \sigma k C(x_0, 0, 0.5\Delta z, t)\Delta t \tag{10}$$

The boundary conditions are $C\big|_{x=x_B} = C\big|_{x=0} = 0$ in the x direction, $C\big|_{y=y_B} = C\big|_{y=0} = 0$ in the y direction, and $\left.\frac{\partial c}{\partial z}\right|_{z=z_B} = \left.\frac{\partial c}{\partial z}\right|_{z=0} = 0$ in the z direction, where the simulation box lies within the spatial region $0 \leq x \leq x_B, 0 \leq y \leq y_B, 0 \leq z \leq z_B$. The equations are solved using a finite-difference scheme, with the explicit Euler method for time integration, and the use of central difference formulae to represent the spatial concentration derivatives. To assist in exploring the parameter space, we can also set a constant stage velocity and have the growth at the leading edge adjust to match that velocity, effectively assuming an arbitrary anisotropic growth rate that allows the ribbon to extend at the appropriate rate relative to the defined width extension rate constant. The final width along the length of the ribbon is saved as the result of the simulation.

Buckingham Π Analysis. A Buckingham Π analysis can reduce the number of relevant variables to a smaller set of physically-motivated, dimensionless variables. From **Table 1**, we see that there are 9 relevant variables in our system. Since there are 3 physical

dimensions (moles, length, and time) amongst the 9 variables, there are 6 dimensionless variables which can be constructed. Applying the analysis to the nannozzle system yields the following recognizable dimensionless groups:

$$\Pi_1 = \frac{k}{D} \tag{11}$$

$$\Pi_2 = \frac{h}{r} \tag{12}$$

$$\Pi_3 = \frac{D}{hv} \tag{13}$$

$$\Pi_4 = \frac{\sigma Q}{k} \tag{14}$$

$$\Pi_5 = \frac{X}{r} \tag{15}$$

$$\Pi_6 = \frac{W}{r} \tag{16}$$

where, Π_1 is the Damköhler number of the system and quantifies the competition between reaction and diffusion, Π_2 is the height to radius ratio of the nanonozzle, Π_3 is the inverse Peclet number, representing the ratio of diffusion velocity and nozzle velocity, Π_4 is the ratio between the molar rates of inflow and consumption, Π_5 is the dimensionless axial coordinate, and Π_6 is the dimensionless width of the growing ribbon. These dimensionless variables should aid in the analysis and interpretation of simulation data, and are used to understand the simulation results later in the paper.

Example Simulation Results. Figure 2 shows an example progression of the simulation, visualizing diffusion from the nozzle and the subsequent growth of the ribbon under conditions where: $\Pi_1 = k/D = 0.2$, $\Pi_2 = h/r = 0.0193$, $\Pi_3 = D/(hv) = 0.0862$, and $\Pi_4 = \sigma Q/k = 562.5$. In the initial pane (Figure 2(a)), the stage has not initiated translation, as the reagent has not yet sufficiently diffused to the ribbon seed below. In the subsequent panes (Figure 2(b)-(d)), the stage translates to match the growth rate of the leading edge of the ribbon, resulting in an elongated island, and ultimately an extended ribbon.

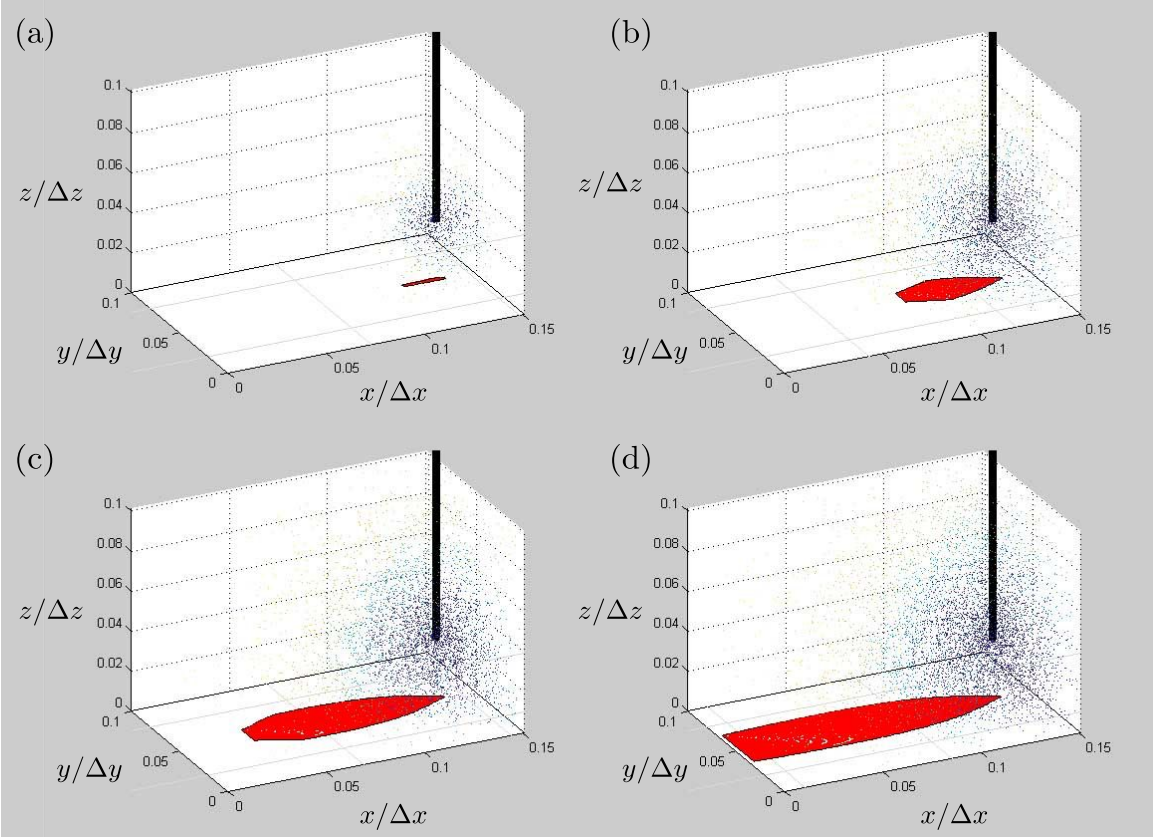

Figure 2. Example progression of diffusion from nanonozzle and nanoribbon growth over time: (a) $t = 200\Delta t$, (b) $t = 400\Delta t$, (c) $t = 600\Delta t$, and (d) $t = 800\Delta t$, where Δt is the timestep of the simulation. Red color on the surface illustrates the monolayer coverage of the ribbon; the black cylinder represents the nanonozzle delivering reagent above the surface; the dot density and color vary as a visualization of a continuous three-

dimensional, gas phase reagent concentration profile. The simulation conditions are: $\Pi_1 = k/D = 0.2$, $\Pi_2 = h/r = 0.0193$, $\Pi_3 = D/(hv) = 0.0862$, and $\Pi_4 = \sigma Q/k = 562.5$.

Formulation of the Ribbon Extension Inequality (REI). An important operational variable for the proposed direct-write scheme is the translation velocity, which must be bounded by the growth rate of the structure. To explore this connection between the translation velocity and the system parameters, we derive a three-dimensional (3D), analytical model to determine the minimum ribbon width possible using the nanonozzle system, because many properties of the ribbon scale with its width, including a quantum confined band gap for the case of graphene. Note that it is very challenging to derive an exact, analytical solution for the nanonozzle system, because it involves the solution to a second-order partial differential equation in three dimensions, coupled with a chemical reaction on a surface, leading to the development of a moving front (the edge of the ribbon). Therefore, to obtain an analytical solution for the system in 3D, we need to make certain assumptions, that will make the problem tractable for solving it exactly. Later in the paper, we evaluate how good these assumptions are by comparing the analytically-obtained solutions for the ribbon width to the numerically-obtained values from the nanonozzle simulations. Accordingly, we assume that the reaction is negligible relative to diffusion, meaning the growth of the ribbon does not influence the concentration profile in the gaseous phase. A first order reaction rate still controls the rate at which the ribbon width increases. For comparison, the Appendix includes solutions for 1D and 2D example models that are simple enough to be solved while including a reaction term for the bulk reactant consumption. Those models indicate that the ratio between reaction and diffusion rates is an important parameter which influences the ribbon width obtained from the nanonozzle.

With the assumption that the gaseous concentration is negligibly decreased by the reaction, we start with the steady-state concentration profile for diffusion from a point source above a surface, given by equation (17) below (this equation can be derived using the well-known method of images[34]). This equation provides an approximate solution for the case of low reaction rate at the surface.

$$C(r,z) = \frac{Q}{4\pi Dh}\left(\frac{1}{\sqrt{\left(z/h - 1\right)^2 + \left(r/h\right)^2}} + \frac{1}{\sqrt{\left(z/h + 1\right)^2 + \left(r/h\right)^2}} \right) \tag{17}$$

where Q is the molar flow rate from the nozzle, D is the diffusion constant, and h is the height of the nozzle outlet above the growth surface. Considering the concentration at the surface ($z = 0$), the equation becomes:

$$C(z=0) = \frac{Q}{2\pi D}\frac{1}{\sqrt{h^2 + r^2}} \tag{18}$$

If we assume that the consumption of the material due to reaction is small relative to the rate at which the material is supplied *via* diffusion, then this equation can be used to calculate the width of the growing nanoribbon. For a first order reaction, the growth rate of the ribbon width, W, can be defined in terms of the concentration profile.

$$\frac{dW}{dt} = 2k_w \sigma C \tag{19}$$

where k_w is the reaction rate constant for growth from a ribbon edge in the width direction and σ is the molar surface area. The factor of two appears because the ribbon extends in

two directions. Assuming the ribbon width is small relative to the length scale of the system, the radial position, r, at the ribbon edge can be simplified to the rectangular coordinate x. Considering the v as a constant velocity for stage translocation to be equal to the rate of change in surface position, dx/dt, the ribbon growth rate can be integrated along length, x, to find the ribbon width at a fixed distance from the nozzle.

$$\int_0^{W_1} dW = \frac{k_w \sigma Q}{\pi D v} \int_0^{X_1} \frac{1}{\sqrt{h^2 + x^2}} dx \tag{20}$$

$$W_1 = \frac{k_w \sigma Q}{\pi D v} \operatorname{arcsinh}\left(X_1 / h \right) \tag{21}$$

In order to grow a continuous ribbon, the velocity at which the stage translates below the nozzle must not exceed the rate at which the ribbon can grow in length from its leading edge. This constraint gives a definition for the maximum velocity in terms of k_l, the rate constant for growth from an edge in the length direction (which is equal to k_w in the case of anisotropic surface growth), and the maximum reagent concentration occurring under the nozzle.

$$v_{\max} = k_l \sigma C\left(r = 0, z = 0\right) \tag{22}$$

$$v_{\max} = \frac{k_l \sigma Q}{2\pi D h} \tag{23}$$

This leads to the governing constraint of the ribbon extension inequality (REI) as:

$$v \le \frac{k_l \sigma Q}{2\pi D h} \tag{24}$$

When programmed into a control algorithm for the translation stage, the REI ensures that the motion of the stage does not exceed the ribbon growth rate. The REI also suggests that direct-write schemes require some real time assessment of the extension rate, or detailed knowledge of the growth kinetics, apart from the usual process parameters. Note that, there could be situations when the motion of the stage exceeds the ribbon growth rate, leading to the formation of a discontinuous ribbon. These are more likely to occur when the nozzle is placed beyond the leading edge of the ribbon. In all our illustrations, including Figure 1(c), we have made it a point to ensure that the nozzle is placed within the leading edge of the ribbon, thereby minimizing the occurrence of discontinuities in the ribbon.

The Minimum Feature Size. As discussed above, the achievable resolution of the direct-write technique is of central interest. Operating at the maximum velocity results in the minimum ribbon width by eliminating excess reaction at the ribbon edges, so this operating state is of particular interest. Applying the definition of v_{max} in equation (23) to the solution for the ribbon width in equation (21) yields the following:

$$W_{1,v\to v_{\max}} = 2h\,\mathrm{arcsinh}\left(X_1 \middle/ h \right) \tag{25}$$

The minimum ribbon width in equation (25) at a fixed distance becomes dependent only on the length scale in the system, the nozzle outlet height, h. It also does not converge to a finite width as $X_1 \to \infty$. To apply this concept practically to a real system, additional phenomena in the system will need to be considered to achieve finite width that is below the minimum described by equation (25). For example, one relevant

approach is to apply local substrate heating to define a more limited reaction zone based on a temperature-sensitive reaction. Another approach is to apply a convective flow to the system or a sweep gas at the periphery of the desired ribbon width, which would allow the concentration, and therefore the reaction rate, to drop off faster than with diffusion alone.

The previously derived analytical expressions can be rewritten in terms of the dimensionless variables identified in equations (11)–(16). The analytical solution for ribbon width, equation (21), rewritten in terms of the dimensionless variables is:

$$\Pi_6 = \frac{\Pi_1^{\,2}\Pi_2\Pi_3\Pi_4}{\pi}\operatorname{arcsinh}\left(\Pi_5 \middle/ \Pi_2\right) \tag{26}$$

Additionally, the definition of the maximum velocity for low reaction rates given by the REI equation (23), which is a requirement of continuous growth, can be rewritten in dimensionless form as follows:

$$\frac{\Pi_1^{\,2}\Pi_3\Pi_4}{2\pi} \geq 1 \tag{27}$$

Effect of the Operating Variables on the Direct-Write Nanonozzle. We are interested in the relationship between the design operating variables and the resulting properties, and use the formulated mathematical model to elucidate these connections. Figure 3 plots the steady-state ribbon width at a fixed distance along the ribbon for a range of different parameters, comparing the results to the analytical solution in equation (21). Panel (a) depicts the ribbon width as a function of the Damköhler number, $\Pi_1 = k/D$. Panel (c)

depicts the ribbon width as a function of the inverse Peclet number, $\Pi_3 = D/(hv)$. Panel (e) depicts the ribbon width as a function of $\Pi_4 = \sigma Q/k$, which represents the competition between the flow rate and consumption. The ribbon width increases as a function of Π_1, Π_3, and Π_4. This is expected because, as the reaction rate increases compared to the diffusion rate, the ribbon can grow to a larger width (panel (a)). Similarly, as the reagent diffusion rate increases compared to the nozzle translation velocity, more material reaches the surface in the time the nozzle covers a fixed distance, leading to a larger ribbon width (panel (c)). Finally, as more material is transported into the system compared to the consumption rate, the ribbon width must increase (panel (e)). Additionally, panels (b), (d), and (f) plot the ratio of the simulated ribbon width to the calculated ribbon width (based on equation (21)), corresponding to the plots in panels (a), (c), and (e), respectively. The closer this ratio is to 1.0, the better is the agreement of the analytical solution with the full simulation.

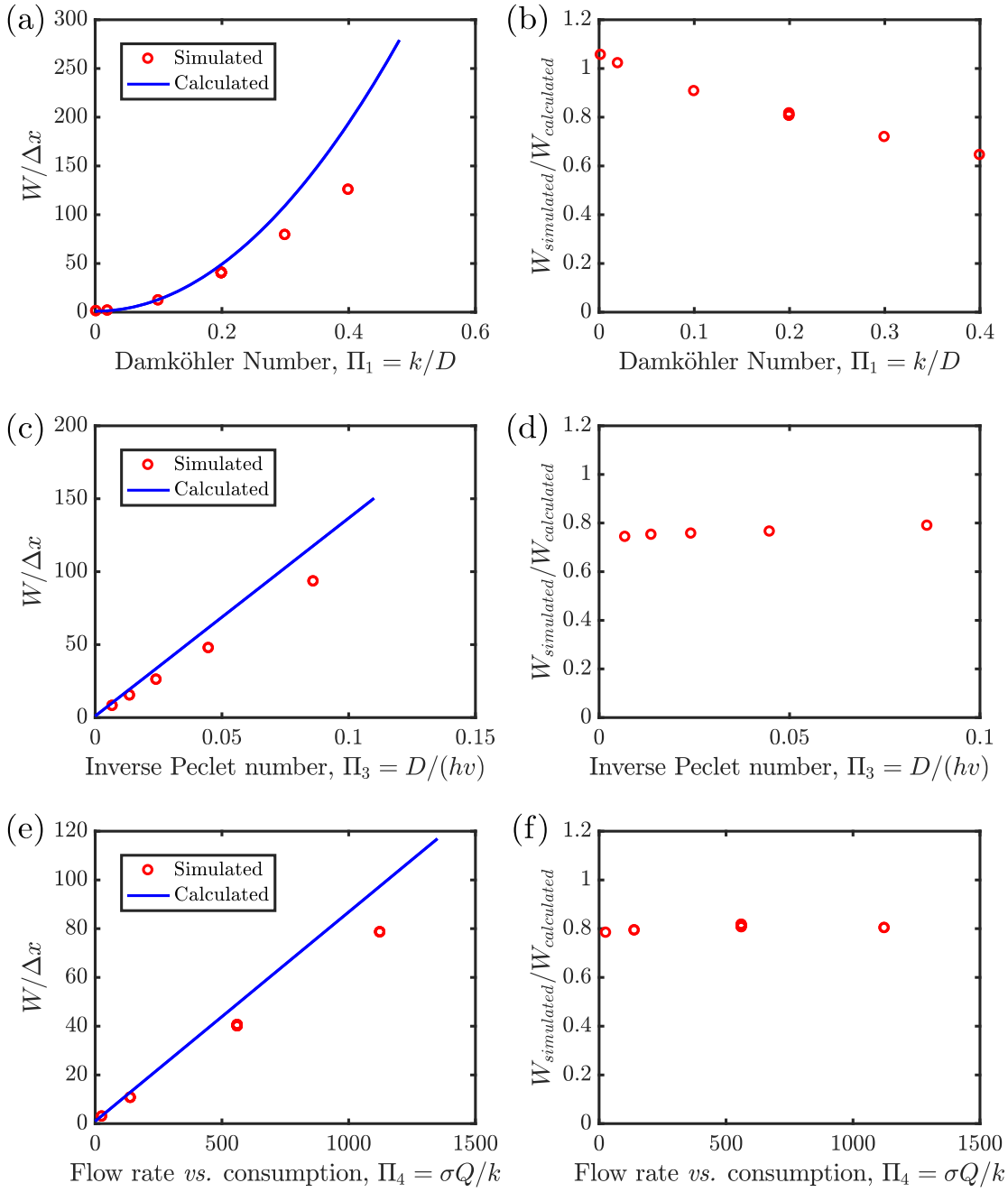

Figure 3: A comparison between the simulated results for ribbon width when varying (a) $\Pi_1 = k/D$, (c) $\Pi_3 = D/(hv)$, and (e) $\Pi_4 = \sigma Q/k$ compared to the calculated analytical solution from equation (21), which is derived in the limit of low reaction rate. The ratio of simulated to calculated ribbon width is also given for (b) Π_1, (d) Π_3, and (f) Π_4. The full parameters and corresponding Π group values of the simulations discussed above are summarized in Table 2 through Table 5.

Checking the Applicability of the Analytical Solution. The primary approximations that were made to justify the derivation of the analytical solution were that: (i) the reaction for ribbon growth does not alter the concentration profile from the no reaction case ($k = 0$), (ii) diffusion occurs from a point source, and (iii) the ribbon width is small relative to the length scale. The first assumption, (i), that the concentration profile is unperturbed by the reaction, is represented by the Damköhler number, $\Pi_1 = k/D$. When Π_1 is low, the reaction rate, *i.e.*, the rate at which material is depleted from the gaseous phase to form the growing ribbon, is low relative to the rate at which diffusion transports material, and the concentration profile is undisturbed. This can be seen in Figure 3(b), where the ratio of the simulated ribbon width to that of the calculated width diverges from 1 at higher Π_1 values. On the other hand, Figure 3(d) demonstrates that, when $\Pi_3 = D/(hv)$, *i.e.*, the inverse Peclet number, is varied, the ratio of the simulated ribbon width to that of the calculated width is nearly independent of Π_3, holding steady around the value expected for the constant value of $\Pi_1 = 0.2$ used in all runs in Figure 3(d). The same holds true for Π_4, as shown in Figure 3(f), in terms of it not being a factor affecting the extent to which the simulations diverge from the analytical calculations.

Approximation (ii) used in deriving the analytical solution, that diffusion occurs from a point source, is valid only if the height of the nozzle outlet above the surface is large relative to the radius of the nozzle outlet, i.e., $\Pi_2 = h/r$ is large. The simulations used values of $\Pi_2 = 19.3$, which justifies approximation (ii). The final approximation, (iii), that the width is small relative to the length scale of the system is more difficult to define distinctly. In the case of an approximate point source, the most appropriate expression is that $\Pi_6/\Pi_2 = W/h$ should be small when $X \sim h$. This value, W/h when $X=h$,

ranges from 0.0001 to 2 in the above simulated results depicted in Figure 3(c) and (d), so it may contribute to the divergence of the simulated results from the calculated for some of the points.

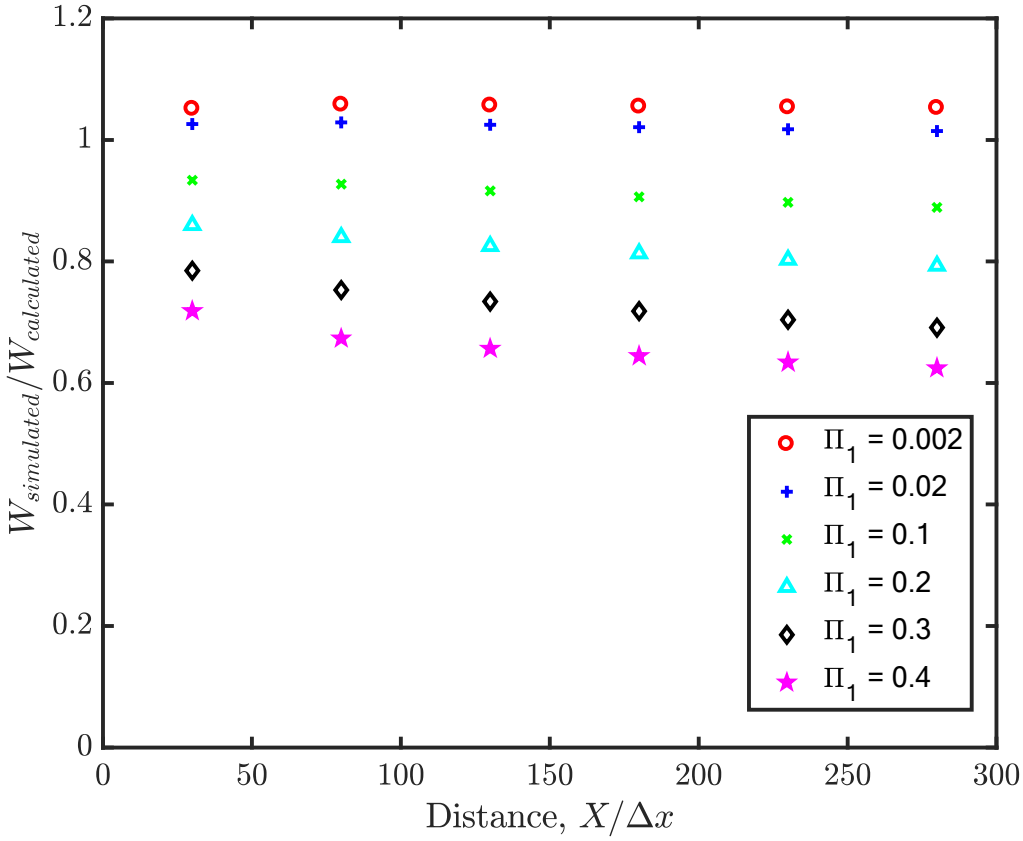

Figure 4. A comparison between the simulated results for ribbon width and the calculated analytical solution from equation (21) when along the length of the simulated ribbon for a range of $\Pi_1 = k/D$, values. Table 2 lists the values of the parameters utilized in the simulations.

The widths reported in Figure 3 occurred at a constant lateral distance, $X/\Delta x$ = 180, from the nozzle. Figure 4 illustrates the ratio of the simulated width to the analytically calculated width along the full length of the simulation for the various Π_1 values shown in Figure 3(b). As shown, the divergence of the simulated results from the

calculated does vary slightly along the length of the ribbon, though not as strongly as the variation with Π_1.

The full parameters and corresponding Π values for the simulations discussed above are summarized in Table 2 through Table 5. Π_1, Π_2, Π_3, and Π_4 are defined as in equations (11)–(14). The box length, width, and height refer to the size of the simulated system. Δx, Δy, Δz denote the voxel size along the length, width, and height dimensions, respectively. Δt denotes the time step size. The nozzle outlet x-, y-, and z-positions refer to the position of the center of the nozzle outlet. The nozzle size sets the length of a side of the nozzle outlet, which is square in shape, thereby determining the spatial positions in the xy plane that are treated as the nozzle outlet defined by equation (2). The variables Q, D, σ, v, and k are defined in **Table 1**.

Table 2. Values of dimensionless variables and simulation parameters for the results depicted in Figure 3(a)–(b).

Condition #	1	2	3	4	5	6	7	8	9	10
Π_1	0.002	0.02	0.1	0.2	0.2	0.2	0.2	0.2	0.3	0.4
Π_2	19.3	19.3	19.3	19.3	19.3	19.3	19.3	19.3	19.3	19.3
Π_3	0.086	0.086	0.086	0.086	0.086	0.086	0.086	0.086	0.086	0.086
Π_4	563	563	563	563	563	563	563	563	563	563
$Q\times10^{11}$	5.63	5.63	5.63	5.63	11.3	5.63	5.63	5.63	5.63	5.63
Box Length / Δx	400	400	400	200	200	400	400	800	400	400
Box Width / Δy	160	160	160	100	100	160	240	240	160	160
Box Height / Δz	70	70	70	60	60	70	90	90	70	70
D	0.001	0.001	0.001	0.001	0.001	0.001	0.001	0.001	0.001	0.001
σ	2×10^{7}	2×10^{8}	1×10^{9}	2×10^{9}	1×10^{9}	2×10^{9}	2×10^{9}	2×10^{9}	3×10^{9}	4×10^{9}
v / ($\Delta x/\Delta t$)	0.4	0.4	0.4	0.4	0.4	0.4	0.4	0.4	0.4	0.4
k	2×10^{-6}	2×10^{-5}	1×10^{-4}	2×10^{-4}	2×10^{-4}	2×10^{-4}	2×10^{-4}	2×10^{-4}	3×10^{-4}	4×10^{-4}

Table 3. Π group values and simulation parameters for the results depicted in Figure 3(c)–(d).

Condition #	11	12	13	14	15
Π_1	0.2	0.2	0.2	0.2	0.2
Π_2	19.3	19.3	19.3	19.3	19.3
Π_3	0.005	0.011	0.022	0.043	0.086
Π_4	1125	1125	1125	1125	1125
$Q\times10^{10}$	1.13	1.13	1.13	1.13	1.13
Box Length / Δx	400	400	400	400	400
Box Width / Δy	240	240	240	240	240
Box Height / Δz	90	90	90	90	90
D	0.001	0.001	0.001	0.001	0.001
σ	2×10^{9}	2×10^{9}	2×10^{9}	2×10^{9}	2×10^{9}
v / ($\Delta x/\Delta t$)	6.4	3.2	1.6	0.8	0.4
k	2×10^{-4}	2×10^{-4}	2×10^{-4}	2×10^{-4}	2×10^{-4}

Table 4. Π group values and simulation parameters for the results depicted in Figure 3(e)–(f).

Condition #	16	17	18	19	20	21	22	23	24	25
Π_1	0.2	0.2	0.2	0.2	0.2	0.2	0.2	0.2	0.2	0.2
Π_2	19.3	19.3	19.3	19.3	19.3	19.3	19.3	19.3	19.3	19.3
Π_3	0.086	0.086	0.086	0.086	0.086	0.086	0.086	0.086	0.086	0.086
Π_4	28	141	141	563	563	563	563	563	563	1125
$Q\times10^{11}$	5.63	1.41	5.63	5.63	11.3	5.63	5.63	5.63	5.63	5.63
Box Length / Δx	400	200	200	200	200	400	400	800	400	400
Box Width / Δy	240	100	100	100	100	160	240	240	240	240
Box Height / Δz	90	60	60	60	60	70	90	90	90	90
D	0.001	0.001	0.001	0.001	0.001	0.001	0.001	0.001	0.001	0.001
σ	1×10^{8}	2×10^{9}	5×10^{8}	2×10^{9}	1×10^{9}	2×10^{9}	2×10^{9}	2×10^{9}	2×10^{9}	4×10^{9}
v / ($\Delta x/\Delta t$)	0.4	0.4	0.4	0.4	0.4	0.4	0.4	0.4	0.4	0.4
k	2×10^{-4}	2×10^{-4}	2×10^{-4}	2×10^{-4}	2×10^{-4}	2×10^{-4}	2×10^{-4}	2×10^{-4}	2×10^{-4}	2×10^{-4}

Table 5. Simulation parameters that are held constant for all results in Figure 3.

Parameter	Value
Δx	0.001
Δy	0.001
Δz	0.001
Δt	0.0001
Nozzle Size / Δx	3
(Nozzle Outlet x-Position) / Δx	20
(Nozzle Outlet y-Position) / (Box Width)	0.5
(Nozzle Outlet z-Position) / Δz	30

Towards Realizing an Experimental Nanonozzle System. Perfecting an experimental nanonozzle system for nanoribbon synthesis and patterning will require precisely controlled instrumentation. However, there are established elements which can provide a starting point; tips for near-field scanning optical microscopy (NSOM) normally provide a conduit for light to pass through an aperture ranging from tens to hundreds of nanometers in diameter, and operate at a distance of tens of nanometers above a surface.[35] Interfacing an NSOM tip with a nanofluidic conduit, instead of light, is an approach that can take advantage of existing technology for controlling a tip at a short distance from a surface. Table 6 utilizes geometric estimates from an NSOM tip along with physical parameters based on graphene and current graphene synthesis to summarize values for the parameters relevant to an experimentally realizable nanonozzle system.

Table 6. Estimates for the values of parameters relevant to an experimentally realizable nanonozzle system.

Variable	Description	SI Units	Estimated Value	Source
D	Diffusion constant	$m^2\ s^{-1}$	10^{-5}	Diffusion of methane in air[36]
k	Edge reaction constant	$m^2\ s^{-1}$	1.0×10^{-6}	Equation (23)

σ	Material area per mass	$m^2\ mol^{-1}$	6.1×10^{-5}	Graphene material property
h	Nozzle outlet height	m	5×10^{-8}	50 nm as achievable height
Q	Reagent flow rate out of nozzle	$mol\ s^{-1}$	8.6×10^{-13}	Hagen–Poiseuille estimate for nozzle flow rate assuming water as a proxy for the reagent, with a pressure drop of 10 atm over a nozzle length of 10 μm
v	Stage translation velocity	$m\ s^{-1}$	1.7×10^{-11}	Target velocity of 1 nm/min
r	Nozzle outlet radius	m	2.5×10^{-8}	Possible NSOM tip aperture around 50 nm

In Table 6, a chemical reaction is assumed to occur with a reagent of similar diffusivity to the currently used common graphene feedstock, methane. We assume a minimum stage velocity of 1 nm/min for a practically viable direct-write system and use equation (23) for the maximum stage velocity to calculate the necessary edge reaction rate, k, of $1.0\times10^{-6}\ m^2\ s^{-1}$ for such a system. This calculated value not only satisfies the approximation made in the derivation of equation (23) that $k/D \ll 1$, but also provides a benchmark for choosing possibly reaction chemistries for an experimental demonstration. From Table 6, it might appear that we have relaxed the assumption that $r \ll h$. However, note that, in equation (23), the radius of the nozzle does not appear explicitly, and only appears indirectly through the reagent flow rate, Q. Accordingly, for a smaller nozzle outlet, the same flow rate Q can be achieved by changing the pressure drop across the NSOM tip. Finally, note that our estimates for the physical variables are in line with previous work utilizing nanosized nozzles. For example, a nanojet with a diameter in the range 50-100 nm, placed at a distance of 50-100 nm from the surface was successfully

utilized as a conduit for microfabrication by pumping neutral, etching radicals towards a solid substrate.[37]

CONCLUSIONS

In this paper, we have introduced a nanonozzle system for direct-write synthesis of a nanostructure (modeled as a nanoribbon) using CVD. The proposed system has the potential to be a novel approach to control the orientation, pitch, and connectivity of nanomaterials on a substrate. Simpler 1D and 2D analytical models reveal the importance of the ratio of reaction and diffusion rates in determining the ribbon width obtained from the nanonozzle. The 3D analytical model provides a simple and reasonably accurate estimation for the expected ribbon width resulting from nanonozzle growth, validated by the more complex nanonozzle simulations, which are based on continuum transport equations. Such simulations would allow the exploration of a wider range of conditions in more advanced models on this topic, exploring additional complexities such as reactions other than first-order, imposed convection, local heating, and other effects that can provide more control over the ribbon width. The presented simulation framework can also be used to provide an estimate of the sensitivity in the system to perturbations in the operating conditions, *e.g.*, examining the non-steady state operation of the nanonozzle as a measure of quality. Future work could also explore the operation of multiple nozzles spaced apart by a suitable distance, so as to grow a periodic array of graphene nanoribbons for large-scale applications, with the most important consideration being preventing the ribbons from merging into each other by using smaller-diameter nanonozzles. To conclude, we hope that the models presented in this

work provide a means for estimating the necessary specifications for experimentally realizing direct-write synthesis *via* a nanonozzle.

CONFLICTS OF INTEREST

The authors have no conflicts of interest to declare.

APPENDIX

We also developed lower dimensional (1D and 2D) analytical models, which highlighted the importance of the consumption term in obtaining a finite width and in determining the minimum width of the possible nanoribbons grown from a nanonozzle. However, in the lower dimensional models this term was defined as a quasi-homogenous reaction, despite the fact that it can only occur at the ribbon edges. To evaluate the feasibility of a nanonozzle system for nanoribbon growth, we performed continuum 3D simulations that more accurately represent the reaction occurring only at the edges of the nanoribbon. In the simple 2D model, the consumption term does not have a rigorous physical definition; it is important to determine whether or not reaction only at the edges is sufficient to yield a finite width nanoribbon, as well as to provide a measure to evaluate the basic correlations implied by the simple models.

1D Model with Diffusion, Convection, and Reaction

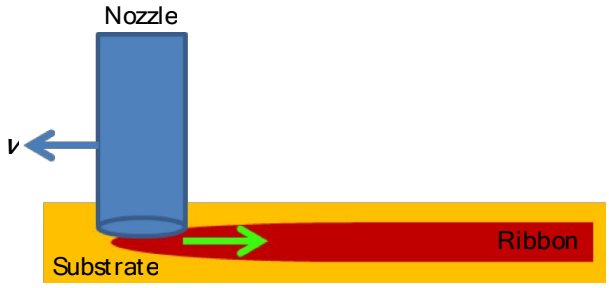

Figure 5. (a) Illustration representing 1D model for nanonozzle growth of a nanoribbon; blue arrow represents nozzle movement with velocity *v*; green arrow represents the diffusion of the reagent in the 1D direction; red bar represents the growing nanoribbon.

At its simplest, the nanonozzle system can be represented by a quasi-1D model, illustrated in Figure 5, where all material leaving the system though a homogeneous reaction term is added to the width. The ribbon width is treated as a variable along the one-dimensional length, but is assumed to be small enough that the 2D nature of the ribbon can be neglected. We consider the reference frame to be the tip of the nozzle, such that the movement of the nozzle can instead be written as a constant convective velocity in the *x*-direction, *v*. For simplicity, the reagent is allowed to diffuse in only one direction away from the nozzle. The 1D convection-diffusion equation in this case is as follows in equation (28):

$$v\frac{dC}{dx} = D\frac{d^2C}{dx^2} - k_w C \tag{28}$$

where C is the 1D concentration, D is the diffusion coefficient, and k_w is the rate constant for a first order reaction representing the growth in width of the nanoribbon. The solution to this equation is given by equation (29), where C_i is the concentration at x=0.

$$C(x) = C_i e^{\frac{v-\sqrt{4Dk_w+v^2}}{2D}x} \tag{29}$$

Note that C_i can alternatively be replaced with a term derived from a constant flow of material from the nanonozzle outlet, n. This alternative form is given by equation (30).

$$C(x) = \frac{n}{\sqrt{k_w\left(D - n/2\sigma\right)}} e^{\frac{v-\sqrt{4Dk_w+v^2}}{2D}x} \tag{30}$$

The growth rate of the width at any given point x can then be described by equation (31), where σ is the areal density of graphene.

$$\frac{dW(x)}{dt} = k_w C(x)\frac{1}{\sigma} \tag{31}$$

To follow a fixed point along the ribbon in time, we account for the moving reference frame by making the substitution $x \rightarrow v\ t$. The expression can then be integrated over time to find the final nanoribbon width, as setup in equation (32) and solved in equation (33), with W_0 representing the minimum width defined by the leading edge of the nanoribbon.

$$W\Big|_{t\to\infty} = W_0 + \int_0^{\infty} \frac{k_w}{\sigma} C(x = vt)\, dt \tag{32}$$

$$W\Big|_{t\to\infty} = W_0 + \frac{C_i}{2\sigma}\left(1 + \sqrt{\frac{4Dk_w}{v^2} + 1}\right) \tag{33}$$

Equation (33) provides a measure of the effect of diffusion on the width of the nanoribbons. In this simple 1D model, all material ends up as part of the nanoribbon, therefore there is a minimum width ($W_0 + C_i / \sigma$) in the limit of no diffusion. However, diffusion can result in a larger width according to the size of the term ($4Dk_w v^{-2}$). Considering that the maximum translation speed of the nanoribbon is the growth rate along the length of the tube, as described by $v = k_\ell C_i/\sigma$, then this term can be rewritten as follows:

$$W\Big|_{t\to\infty} = W_0 + \frac{C_i}{2\sigma}\left(1 + \sqrt{\frac{4Dk_w\sigma^2}{(k_\ell C_i)^2} + 1}\right) \tag{34}$$

Assuming that $k = k_\ell = 0.5\ k_w$, *i.e.*, the growth rate at the edge for both the width and the length is the same (accounting for the fact two edges are associated with growth of the width), equation (34) can be further simplified in the limit of low concentration, as shown in equation (35):

$$W\Big|_{\substack{t\to\infty \\ C_i\to 0}} = W_0 + \sqrt{\frac{2D}{k}} \tag{35}$$

This form highlights that the ratio of diffusion to reaction is what controls the minimum achievable width, which will be shown again the next model as well.

2D Model with Diffusion and Reaction

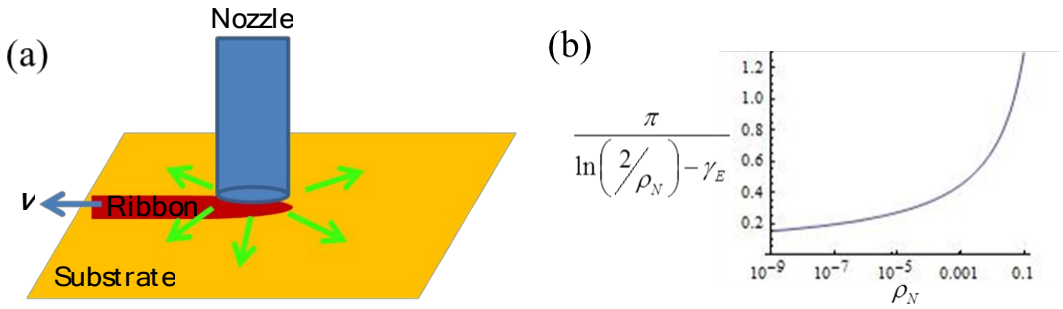

Figure 6. (a) Illustration representing 2D model for nanonozzle growth of a nanoribbon; the blue arrow represents stage movement; the green arrows represent diffusion of reagent in the 2D plane of the substrate; the red bar represents growing nanoribbon. (b) Semi-log plot of component in equation (44) for nanoribbon width that is determined by the non-dimensionalized nanonozzle size, ρ_N.

Though simple, the 1D model is quite removed from a physical system. A 2D model, illustrated in **Figure 6**(a), adds back some of the complexity. In a 2D perspective, reagent leaves the nanonozzle and spreads out *via* diffusion in a plane, with the motion of the nozzle relative to the substrate acting as an effective convection term. This full 2D case becomes too complex for an analytical solution; however, considering the case where convection is negligible and adding a first order consumption term across the entire surface, not only at the ribbon edge, yields usable results.

Ignoring convective terms appears to be a reasonable simplification under the assumption that the growth rate will be similar to the rates of current CVD growth processes for graphene, which advance at a rate of order 1 μm/min.[12,38] Comparing this to diffusion coefficients in air, which are of order 10^{-6} m^2/s, reveals that the Peclet

number, the ratio of convective to diffusive contributions, is negligible at length scales smaller than ~10 m, and can therefore be ignored as we are considering length scales on the order of nanometers. The inclusion of a first order bulk consumption term is not as readily justified. From the perspective or diffusion on a surface, the consumption term can be considered the rate at which reagent desorbs from the surface and is lost. It can also be considered a proxy term to represent mass that forms the nanoribbon. By including this term without rigorously justifying these perspectives, we will only use the results drawn from this model as qualitative observations that inform the direction for more advanced models.

Based on the assumptions listed above, the differential equation can be simplified in radial coordinates to yield equation (36), where k_{-A} is the rate constant of the first order consumption term.

$$\frac{D}{r}\frac{\partial}{\partial r}\left(r\frac{\partial C}{\partial r}\right)-k_{-A}C=0 \tag{36}$$

The solution is described by equation (37), with A as a constant to be defined by the boundary condition, K_0 being the modified Bessel function of the 2nd kind, and ρ as non-dimensionalized radius.

$$C(r)=AK_0\left(\frac{r}{\sqrt{D/k_{-A}}}\right)=AK_0\left(\rho\right) \tag{37}$$

The boundary condition (BC) is defined in equation (38) as a constant flux outwards at the dimensionless nanonozzle radius, ρ_N:

$$\text{BC:} \quad n = -2\pi \rho_N D \left.\frac{dC}{d\rho}\right|_{\rho_N} \tag{38}$$

As done previously, tracking the width at a given point on the substrate can be related to an integral along the length, as defined in equation (39):

$$W = W_0 + \int_{\rho_N}^{\infty} \frac{k_w}{v\sigma} A K_0(\rho) \sqrt{D/k_{-A}}\, d\rho \tag{39}$$

In this case, there is no general analytical solution with a simple form. However, making the assumption that ρ_N, the nanonozzle radius, is small, the simplifications described by equations (40) to (44) are possible:

$$\lim_{\rho_N \to 0} \int_{\rho_N}^{\infty} K_0(\rho) d\rho = \pi/2 \tag{40}$$

$$\lim_{\rho_N \to 0} A = \frac{n}{2\pi D} \tag{41}$$

$$\lim_{\rho_N \to 0} C(\rho_N) \approx \frac{n}{2\pi D}\left(\ln\left(2/\rho_N\right) - \gamma_E\right) + O\left(\rho^2\right) \tag{42}$$

$$\lim_{\rho_N \to 0} W = W_0 + \frac{n k_w \omega}{4v\sqrt{D k_{-A}}} = W_0 + \frac{n}{2C(\rho_N)\sqrt{D k_{-A}}} \tag{43}$$

$$\lim_{\rho_N \to 0} W = W_0 + \sqrt{\frac{D}{k_{-A}}} \frac{\pi}{\ln\left(2/\rho_N\right) - \gamma_E} \tag{44}$$

where γ_E is Euler's constant. The combined value of the numeric terms in equation (44) is plotted in **Figure 6**(b). An important observation from the result of this limit is that the flow out of the nozzle cancels out of the final expression for width. This removes an intuitive parameter to control growth, and emphasizes the importance of the length scale defined by the ratio of diffusion to reaction rate. In practice, the width can always be made larger by operating at a lower velocity than the maximum possible, but the minimum width is strictly defined by the transport and chemical properties.

REFERENCES

(1) Garno, J. C.; Yang, Y.; Amro, N. A.; Cruchon-Dupeyrat, S.; Chen, S.; Liu, G.-Y. Precise Positioning of Nanoparticles on Surfaces Using Scanning Probe Lithography. *Nano Lett.* **2003**, *3*, 389–395.

(2) Chiu, J. J.; Kim, B. J.; Kramer, E. J.; Pine, D. J. Control of Nanoparticle Location in Block Copolymers. *J. Am. Chem. Soc.* **2005**, *127*, 5036–5037.

(3) Fresco, Z. M.; Fréchet, J. M. J. Selective Surface Activation of a Functional Monolayer for the Fabrication of Nanometer Scale Thiol Patterns and Directed Self-Assembly of Gold Nanoparticles. *J. Am. Chem. Soc.* **2005**, *127*, 8302–8303.

(4) Aldaye, F. A.; Palmer, A. L.; Sleiman, H. F. Assembling Materials with DNA as the Guide. *Science* **2008**, *321*, 1795–1799.

(5) Drexler, K. E. Productive Nanosystems: The Physics of Molecular Fabrication. *Phys. Educ.* **2005**, *40*, 339–346.

(6) Drexler, K. E.; Randall, J.; Corchnoy, S.; Kawczak, A.; Steve, M. L. Productive Nanosystems: A Technology Roadmap. **2007**.

(7) Integrated Nanosystems for Atomically Precise Manufacturing Workshop – August 5-6, 2015, Energy Efficiency & Renewable Energy, U.S. Department of Energy https://energy.gov/eere/amo/downloads/integrated-nanosystems-atomically-precise-manufacturing-workshop-august-5-6-2015.

(8) Son, Y.-W.; Cohen, M. L.; Louie, S. G. Energy Gaps in Graphene Nanoribbons. *Phys. Rev. Lett.* **2006**, *97*, 216803.

(9) Chen, Y.-C.; de Oteyza, D. G.; Pedramrazi, Z.; Chen, C.; Fischer, F. R.; Crommie, M. F. Tuning the Band Gap of Graphene Nanoribbons Synthesized from Molecular Precursors. *ACS Nano* **2013**, *7*, 6123–6128.

(10) Jiao, L.; Zhang, L.; Wang, X.; Diankov, G.; Dai, H. Narrow Graphene Nanoribbons from Carbon Nanotubes. *Nature* **2009**, *458*, 877–880.

(11) Ito, T.; Okazaki, S. Pushing the Limits of Lithography. *Nature* **2000**, *406*, 1027–1031.

(12) Jacobberger, R. M.; Kiraly, B.; Fortin-Deschenes, M.; Levesque, P. L.; McElhinny, K. M.; Brady, G. J.; Rojas Delgado, R.; Singha Roy, S.; Mannix, A.; Lagally, M. G.; Evans, P. G.; Desjardins, P.; Martel, R.; Hersam, M. C.; Guisinger, N. P.; Arnold, M. S. Direct Oriented Growth of Armchair Graphene Nanoribbons

on Germanium. *Nat. Commun.* **2015**, *6*, 8006.

(13) Moreau, W. M. *Semiconductor Lithography: Principles, Practices, and Materials*; Springer Science & Business Media, 2012.

(14) Manfrinato, V. R.; Stein, A.; Zhang, L.; Nam, C.-Y.; Yager, K. G.; Stach, E. A.; Black, C. T. Aberration-Corrected Electron Beam Lithography at the One Nanometer Length Scale. *Nano Lett.* **2017**, *17*, 4562–4567.

(15) Wang, M. C. P.; Gates, B. D. Directed Assembly of Nanowires. *Mater. Today* **2009**, *12*, 34–43.

(16) Lee, W.-K.; Whitman, L. J.; Lee, J.; King, W. P.; Sheehan, P. E. The Nanopatterning of a Stimulus-Responsive Polymer by Thermal Dip-Pen Nanolithography. *Soft Matter* **2008**, *4*, 1844.

(17) Hua, Y.; King, W. P.; Henderson, C. L. Nanopatterning Materials Using Area Selective Atomic Layer Deposition in Conjunction with Thermochemical Surface Modification via Heated AFM Cantilever Probe Lithography. *Microelectron. Eng.* **2008**, *85*, 934–936.

(18) Funke, J. J.; Dietz, H. Placing Molecules with Bohr Radius Resolution Using DNA Origami. *Nat. Nanotechnol.* **2015**, *11*, 47–52.

(19) José-Yacamán, M.; Miki-Yoshida, M.; Rendón, L.; Santiesteban, J. G. Catalytic Growth of Carbon Microtubules with Fullerene Structure. *Appl. Phys. Lett.* **1993**, *62*, 657–659.

(20) Reina, A.; Jia, X.; Ho, J.; Nezich, D.; Son, H.; Bulovic, V.; Dresselhaus, M. S.;

Kong, J. Large Area, Few-Layer Graphene Films on Arbitrary Substrates by Chemical Vapor Deposition. *Nano Lett.* **2009**, *9*, 30–35.

(21) Hampden-Smith, M. J.; Kodas, T. T. Chemical Vapor Deposition of Metals: Part 1. An Overview of CVD Processes. *Chem. Vap. Depos.* **1995**, *1*, 8–23.

(22) Dhanasekaran, R. Growth of Semiconductor Single Crystals from Vapor Phase. In *Springer Handbook of Crystal Growth*; Springer Berlin Heidelberg: Berlin, Heidelberg, 2010; pp. 897–935.

(23) Vieu, C.; Carcenac, F.; Pépin, A.; Chen, Y.; Mejias, M.; Lebib, A.; Manin-Ferlazzo, L.; Couraud, L.; Launois, H. Electron Beam Lithography: Resolution Limits and Applications. *Appl. Surf. Sci.* **2000**, *164*, 111–117.

(24) Chen, Y. Nanofabrication by Electron Beam Lithography and Its Applications: A Review. *Microelectron. Eng.* **2015**, *135*, 57–72.

(25) Han, M. Y.; Özyilmaz, B.; Zhang, Y.; Kim, P. Energy Band-Gap Engineering of Graphene Nanoribbons. *Phys. Rev. Lett.* **2007**, *98*, 206805.

(26) Salaita, K.; Wang, Y.; Mirkin, C. A. Applications of Dip-Pen Nanolithography. *Nat. Nanotechnol.* **2007**, *2*, 145–155.

(27) Smith, P. A.; Nordquist, C. D.; Jackson, T. N.; Mayer, T. S.; Martin, B. R.; Mbindyo, J.; Mallouk, T. E. Electric-Field Assisted Assembly and Alignment of Metallic Nanowires. *Appl. Phys. Lett.* **2000**, *77*, 1399–1401.

(28) Hangarter, C. M.; Myung, N. V. Magnetic Alignment of Nanowires. *Chem. Mater.* **2005**, *17*, 1320–1324.

(29) Rothemund, P. W. K. Folding DNA to Create Nanoscale Shapes and Patterns. *Nature* **2006**, *440*, 297–302.

(30) Gothelf, K. V.; Tørring, T. DNA Nanotechnology: A Curiosity or a Promising Technology? *F1000Prime Rep.* **2013**, *5*.

(31) Voigt, J.; Shi, F.; Edinger, K.; Güthner, P.; Rangelow, I. W. Nanofabrication with Scanning Nanonozzle 'Nanojet.' *Microelectron. Eng.* **2001**, *57–58*, 1035–1042.

(32) Goto, M.; Zhigilei, L. V.; Hobley, J.; Kishimoto, M.; Garrison, B. J.; Fukumura, H. Laser Expulsion of an Organic Molecular Nanojet from a Spatially Confined Domain. *J. Appl. Phys.* **2001**, *90*, 4755–4760.

(33) Fogler, H. S. *Elements of Chemical Reaction Engineering*; Prentice-Hall, Inc.: Upper Saddle River, N.J., 1999.

(34) Deen, W. M. *Analysis of Transport Phenomena*; Oxford University Press, 2011.

(35) Dunn, R. C. Near-Field Scanning Optical Microscopy. *Chem. Rev.* **1999**, *99*, 2891–2928.

(36) Marrero, T. R.; Mason, E. A. Gaseous Diffusion Coefficients. *J. Phys. Chem. Ref. Data* **1972**, *1*, 3–118.

(37) Rangelow, I. W.; Voigt, J.; Edinger, K. "NANOJET": Tool for the Nanofabrication. *J. Vac. Sci. Technol. B Microelectron. Nanom. Struct.* **2001**, *19*, 2723.

(38) Li, X.; Magnuson, C. W.; Venugopal, A.; Tromp, R. M.; Hannon, J. B.; Vogel, E.

M.; Colombo, L.; Ruoff, R. S. Large-Area Graphene Single Crystals Grown by Low-Pressure Chemical Vapor Deposition of Methane on Copper. *J. Am. Chem. Soc.* **2011**, *133*, 2816–2819.

TOC Graphic